Supporting Information: Twistronics in tensile strained bilayer black phosphorus

Peng Kang,*,†,‡ Wanting Zhang,† Vincent Michaud-Rioux,† Xin Wang,† Jiangni Yun,‡ and Hong Guo†

†*Center for the Physics of Materials and Department of Physics, McGill University, Montreal, Quebec H3A 2T8, Canada*

‡*School of Information Science and Technology, Northwest University, Xi'an 710127, People's Republic of China*

E-mail: kangp@physics.mcgill.ca

In the Supporting Information, we provide relevant technical details of the calculation reported in the main text as well as supporting data.

Geometric information of tbBPs

Table S1: Structural information of all tbBPs. The lattice mismatch is defined by the supercell length along the x- and y-directions ($L_{x,y}^{tBP,uBP}$) as $M_{tbBP} \equiv [(L_x^{tBP} - L_x^{uBP})/L_x^{tBP} + (L_y^{tBP} - L_y^{uBP})/L_y^{tBP}]/2$, where superscripts *tBP* and *uBP* mean twisted and untwisted BP of two constituent monolayers, respectively.

	Twisted Bilayer Black Phosphorus				
Twist Angle	$\theta = 1.8^\circ$	$\theta = 2.2^\circ$	$\theta = 2.7^\circ$	$\theta = 3.6^\circ$	$\theta = 5.4^\circ$
Number of atoms	8068	5604	3588	2020	900
$n \times p$	24×42	20×35	16×28	12×21	8×14
Supercell size (Å)	140.70×106.35	117.25×88.63	93.90×70.98	70.35×53.17	47.00×35.35
Lattice mismatch M_{tbBP}	0.049 %	0.071 %	0.111 %	0.198 %	0.443 %

The geometric information of all five tbBPs are listed in Table S1, as the same as listed in

Table 1 of the main text. The untwisted BP, which is one of the two constituent monolayer BPs, is formed by expanding the primitive cell of BP (AA stacking) with a factor of p and n along the x and y directions respectively. The twisted monolayer BP is formed by rotating the uBP by an angle θ. Plus, the schematic plots of atomic structures of all five tbBP configurations are presented as Figure S1. For more details we refer interested readers to our previous work.[1]

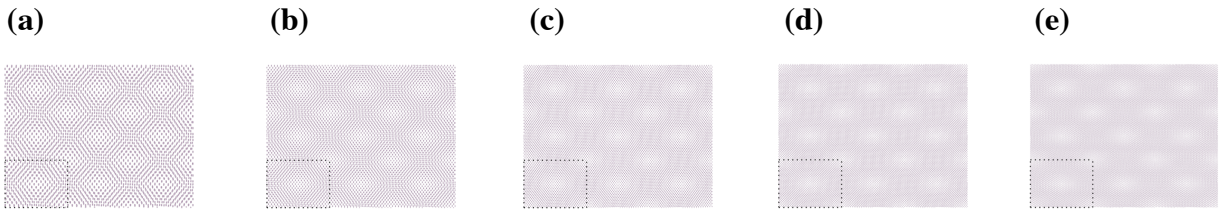

Figure S1: The schematic plots of atomic structures of twisted bilayer black phosphorus with twist angle (a) $\theta = 5.4^\circ$, (b) $\theta = 3.6^\circ$, (c) $\theta = 2.7^\circ$, (d) $\theta = 2.2^\circ$ and (e) $\theta = 1.8^\circ$.

For the detailed model constructions of supercell of tbBPs, we would like to describe it as follow. First of all, we build a primitive cell of monolayer black phosphorus (the small black rectangle in Figure S2, namely uBP) associated with lattice constant a and b. Once it's done, both directions of lattice vectors are re-oriented with angle θ and a new supercell of monolayer black phosphorus (large red rectangle in Figure S2, namely tBP) is constructed. As a result, the twist angle θ could be calculated by

$$\theta = arctan\frac{a}{nb} = arctan\frac{b}{pa} \tag{1}$$

after the transformation, we could have

$$\frac{a^2}{b^2} = \frac{n}{p} \tag{2}$$

where n and p are both integer 1, 2, 3,.... Since $a^2/b^2 \approx 4/7$, in order to make sure that the twist angles are small enough, the factors (n, p) are chosen as (24, 42), (20, 35), (16, 28), (12, 21), (8, 14) corresponding to twist angle $\theta = 1.8^\circ$, 2.2°, 2.7°, 3.6° and 5.4°, respectively.

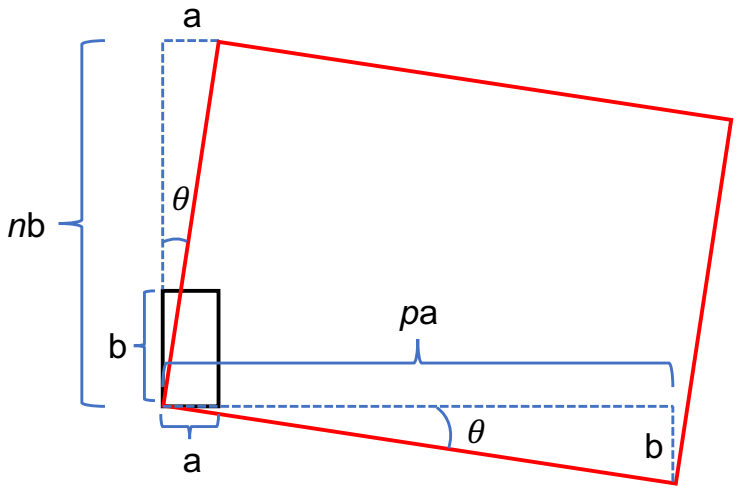

Figure S2: The illustration of supercell construction of twisted bilayer black phosphorus.

Mechanical properties of tbBPs

In this section, we summarized the calculated mechanical properties of all tbBPs, AA stacking bilayer BP and monolayer BP, including elastic stiffness constants, ultimate tensile stress and strain, presented in Table S2. In addition, as an example, the schematic plot of atomic structural several snapshots of 2.7-tbBP configuration under elastic (3.5%), plastic (10% and 12.5%) and fracture deformation (13%, 13.5% and 14%) are shown in Figure S3.

In order to well simulate the atomic volume, we have applied the periodic boundary conditions in both armchair and zigzag directions while the free surface boundary condition is adopted in the out-of-plane direction. Generally, the atomic stress of each atom in the simulation system is calculated according to the equation[2]

$$\Omega^{\alpha}\sigma_{ij}^{\alpha} = \frac{1}{2}m^{\alpha}\upsilon_{i}^{\alpha}\upsilon_{j}^{\alpha} + \sum_{\beta=1,n} r_{\alpha\beta}^{j} f_{\alpha\beta}^{i} \tag{3}$$

where i and j denote indices in the Cartesian coordinate system; α and β are the atomic indices while m^{α} and υ^{α} indicate the mass and velocity of atom α; $r_{\alpha\beta}$ and $f_{\alpha\beta}$ are the distance and force between atoms α and β, respectively; and Ω^{α} is the atomic volume of atom α. Furthermore, we

simulate the stress-strain by averaging the total atomic stress over the volume of the system as

$$\frac{\sum_\alpha \Omega^\alpha \sigma_{ij}^\alpha}{V} = \frac{\sum_\alpha \left(\frac{1}{2} m^\alpha v_i^\alpha v_j^\alpha + \sum_{\beta=1,n} r_{\alpha\beta}^j f_{\alpha\beta}^i\right)}{V} \tag{4}$$

where V is the volume of the system. Here, the thickness of monolayer BP is taken as 5.24 Å [3,4] in the computation of the system volume regarding the stress-strain relations.

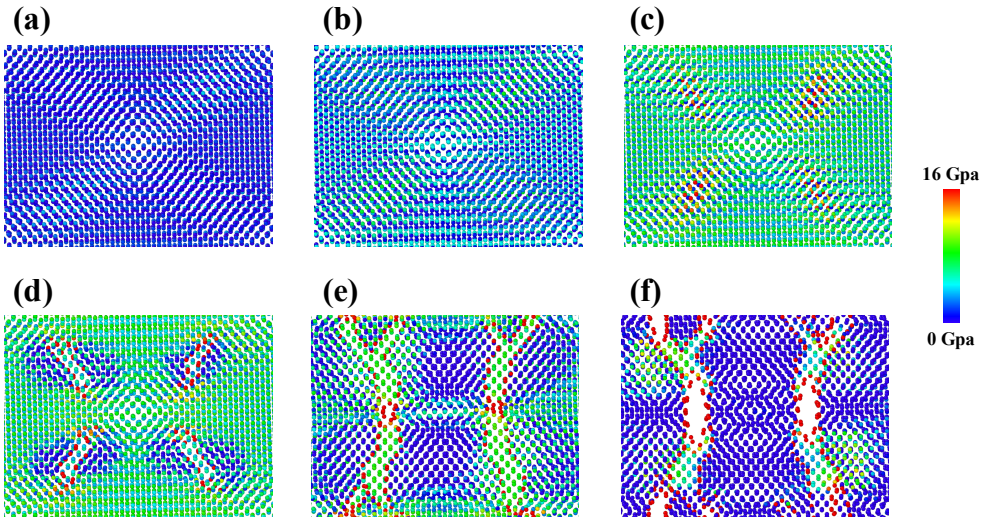

Figure S3: The atomic structures of 2.7-tbBP with tensile deformation of (a) 3.5%, (b) 10 %, (c) 12.5%, (d) 13%, (e) 13.5%, and (f) 14% along x-direction. The stress distribution of atomic configurations during fracture failure process are colour coded at right side.

Table S2: The calculated mechanical properties of all tbBPs, AA stacking bilayer BP and monolayer BP. The unit of elastic stiffness constants and ultimate tensile stress is GPa.ZZ and AC represent the zigzag and armchair directions, respectively.

	Elastic stiffness constants		Ultimate tensile stress		Ultimate tensile strain	
	ZZ	AC	ZZ	AC	ZZ	AC
1.8-tbBP	152	58	12.5	6.8	0.128	0.230
2.2-tbBP	154	58	12.5	6.7	0.130	0.233
2.7-tbBP	161	63	12.2	6.8	0.127	0.242
3.6-tbBP	158	62	13.2	7.0	0.131	0.246
5.4-tbBP	157	62	12.7	6.9	0.138	0.251
Bilayer BP (AA-stacking)	121	45	12.1	6.5	0.209	0.311
Monolayer BP	113	41	11.4	6.1	0.205	0.308

Carrier mobility calculation of tensile deformed 3.6-tbBP

The hole carrier mobility μ_h along armchair direction in uniaxial tensile deformed 3.6-tbBP are calculated by applying deformation potential theory[5] with crossover function[6]

$$\mu_{film} = \frac{\pi e \hbar^4 C_{film}}{\sqrt{2}(k_B T)^{3/2}(m^*)^{5/2}(D_A)^2} \cdot F \tag{5}$$

where F is a crossover function that bridges 2D and 3D,

$$F \equiv \frac{\sum_n \{\frac{\sqrt{\pi}}{2}[1-\mathrm{erf}(\Omega(n)] + \Omega(n) e^{-\Omega^2(n)}\}}{\sum_n [1+\Omega^2(n)] e^{-\Omega^2(n)}} \tag{6}$$

and

$$\Omega(n) \equiv \sqrt{\frac{n^2\pi^2\hbar^2}{2m^* {W_{eff}}^2 k_B T}} .$$

In the crossover function F, erf is the error function, the summation over integers n is due to quantum confinement along the z-direction (finite thickness direction) and W_{eff} can be calculated using the wave functions obtained by KS-DFT or analytically assuming a square-well confinement potential. In Eq. (5), D_A is the deformation potential which is defined as $\delta E_i = D_{Ai}\delta a/a$, where δE_i is the energy change of the i^{th} electronic band under proper cell compression and dilatation with respect to the equilibrium cell and a is the lattice constant and δa the deformation of a. C_{film} is related to the calculated elastic stiffness constants extracted from stress-strain relation. m^* is the calculated effective mass, extracted from calculated band structures along the transport (armchair) direction. The supercell dilation or compression (e.g. deformation) proceeds by increments of 0.5 % in the subsequent KS-DFT calculations.

Here, for the hole carrier mobility calculation of uniaxial tensile deformed 3.6-tbBP, the hole effective mass m_h^* are extracted from calculated band structures of each tensile deformed atomic configurations of 3.6-tbBP, while the deformation potential D_A and elastic stiffness constants C_{film} are adapted from the prediction of equilibrium 3.6-tbBP. The previous calculations[7] denote that it is a plausible method for preforming carrier mobility of strained materials. The calculated values

of D_A, C_{film}, m_h^* and hole carrier mobility μ_h are presented in Table S3.

Table S3: Calculated effective mass m^* in units of bare mass m_0, elastic stiffness C_{film} in units of GPa, deformation potential D_A in units of eV and mobility μ in units of $cm^2V^{-1}s^{-1}$ for the 3.6-tbBPs along the armchair (y) direction, corresponding to the Γ-Y direction in the 2D Brillouin zone. The subscript h (hole) indicates the carrier type.

Tensile deformed direction	Strain	m_h^*	C_{film}	D_A	μ_h
Zigazag direction	1 %	0.162	62	3.07	4901
	2 %	0.171			4387
	3 %	0.186			3703
	4 %	0.201			3134
	6 %	0.239			2214
	8 %	0.305			1321
	10 %	0.504			438
	12 %	2.09			23
Armchair direction	2 %	0.164	62	3.07	4783
	4 %	0.175			4169
	6 %	0.185			3611
	8 %	0.194			3387
	10 %	0.201			3102
	14 %	0.211			2814
	18 %	0.216			2720
	22 %	0.218			2693
	24.8 %	0.220			2621

Negative Poisson's ratio in tbBPs

The effect of in-plane negative Poisson's ratio (NPR), where transverse direction extend as longitudinal tensile loading is applied, is demonstrated in tbBPs. Here, the Poisson's ratio is calculated by its definition

$$\nu = \frac{\varepsilon_r}{\varepsilon_a} \tag{7}$$

where ε_a is applied tensile strain along one direction and ε_a is the resultant strain along the other direction. The corresponding results of NPR are plotted in Figure S4. The effect of NPR is discovered during armchair tensile deformation in 3.6-tbBP, as indicated in Figure S4(c) and the same

observations are also presented in all five tbBPs, as shown in Figure S4(d). The NPR is demonstrated as the armchair tensile strain up to 0.20 $\sim$ 0.22 for all tbBPs. The origin of this effect could be mostly understood from two aspects: First, due to the coexistence of four high-symmetry stacking configurations in tbBPs, the corrugation perpendicular to 2D plane is constructed in equilibrium tbBPs and it undergoes a de-wrinkling process so as to assume a more planar conformation resulting in an in-plane NPR, which is the 'wrinkled paper model'. Second, the geometric puckered structures and coupled hinge-like bonding configurations in few-layer BP could result in this phenomenon, which has been investigated in previous work.[8–11]

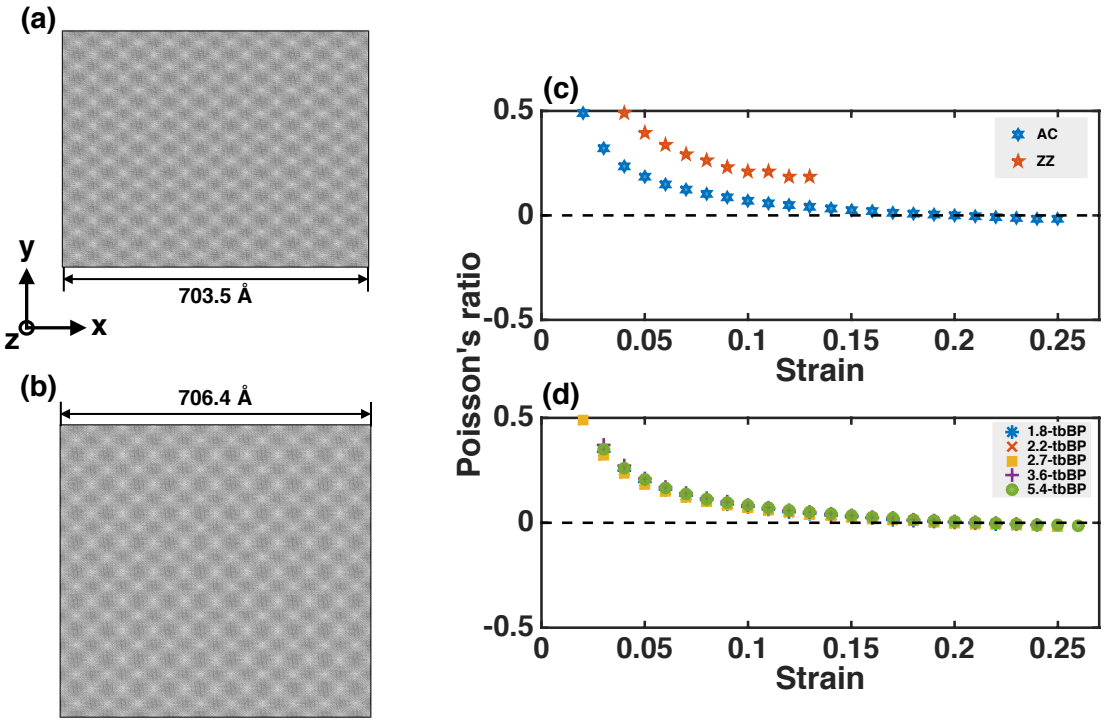

Figure S4: The schematic plot of 3.6-tbBP (10 times replication of supercell along x and y direction) with (a) no deformation and (b) 0.25 armchair tensile deformation (y-direction). The scale in resultant zigzag direction (x-direction) is 706.4 Åwith 0.25 armchair tensile deformation, larger than 703.5 Åwith no deformation, indicating the effect of NPR. (c) The Poisson's ration as a function of armchair (AC) and zigzag (ZZ) tensile strain in 3.6-tbBP. (d) The Poisson's ration as a function of zigzag (ZZ) tensile strain in all five tbBPs.

References

(1) Kang P, Zhang W T, Michaud-Rioux V, et al. Moiré impurities in twisted bilayer black phosphorus: Effects on the carrier mobility[J]. Physical Review B, 2017, 96(19): 195406.

(2) Chandra N, Namilae S, Shet C. Local elastic properties of carbon nanotubes in the presence of Stone-Wales defects[J]. Physical Review B, 2004, 69(9): 094101.

(3) Li L, Yang J. On mechanical behaviors of few-layer black phosphorus[J]. Scientific Reports, 2018, 8(1): 1-8.

(4) Jiang J W. Parametrization of Stillinger–Weber potential based on valence force field model: application to single-layer MoS2 and black phosphorus[J]. Nanotechnology, 2015, 26(31): 315706.

(5) Bardeen J, Shockley W. Deformation potentials and mobilities in non-polar crystals[J]. Physical Review, 1950, 80(1): 72.

(6) Kang P, Michaud-Rioux V, Kong X H, et al. Calculated carrier mobility of h-BN/-InSe/h-BN van der Waals heterostructures[J]. 2D Materials, 2017, 4(4): 045014.

(7) Wu M, Shi J, Zhang M, et al. Enhancement of photoluminescence and hole mobility in 1-to 5-layer InSe due to the top valence-band inversion: strain effect[J]. Nanoscale, 2018.

(8) Du Y, Maassen J, Wu W, et al. Auxetic black phosphorus: a 2D material with negative Poisson's ratio[J]. Nano Letters, 2016, 16(10): 6701-6708.

(9) Jiang J W, Rabczuk T, Park H S. A Stillinger–Weber potential for single-layered black phosphorus, and the importance of cross-pucker interactions for a negative Poisson's ratio and edge stress-induced bending[J]. Nanoscale, 2015, 7(14): 6059-6068.

(10) Jiang J W, Park H S. Negative poisson's ratio in single-layer black phosphorus[J]. Nature Communications, 2014, 5: 4727.

(11) Ho D T, Ho V H, Park H S, et al. Negative InPlane Poisson's Ratio for Single Layer Black Phosphorus: An Atomistic Simulation Study[J]. Physica Status Solidi (b), 2017, 254(12): 1700285.